Mechanism of the *fcc–hcp* Phase Transformation in Solid Ar

Bingxi Li,[1,*] Guangrui Qian,[2] Artem R. Oganov,[2] Salah Eddine Boulfelfel,[3] and Roland Faller[4,†]

[1] *Department Materials Science and Engineering, University of California, Davis, CA 95616, USA*
[2] *Department of Geosciences, Stony Brook University, Stony Brook, NY 11794, USA*
[3] *School of Chemical and Biomolecular Engineering, Georgia Institute of Technology, Atlanta, GA 30332, USA*
[4] *Department of Chemical Engineering, University of California, Davis, CA 95616, USA*

(Dated: March 17, 2016)

We present an atomistic description of the mechanism of the *fcc*–to–*hcp* transformation in solid argon obtained from molecular dynamics transition path sampling simulations. We show that the transition barrier at 40 K under ambient pressure is close to the thermal energy per atom. The analysis of the ensemble of reactive trajectories collected during the sampling revealed three transition types. The average coordination number is used as order parameter and to monitor the progress of the transformation. In each transition type, under– and over–coordinated atoms form and distribute uniformly throughout the lattice during the transformation. Stacking disorder is discussed to describe the transition process and the cooperative atomic motions. The high activation energy for collective movements of many atoms explains previous experimental observations of a sluggish bulk transformations and difficulties of observation of the bulk transition at lower temperature and ambient pressure. The transition mechanism in bulk Ar is different from Ar clusters as the orthorhombic intermediate structure proposed for the latter is not observed.

I. INTRODUCTION

Rare gas solids (neon, argon, krypton, xenon) crystallize in face–centered cubic (*fcc*) structures at ambient pressure and low temperatures[1,2]. However, early experimental studies and theoretical predictions pointed out the possibility of a hexagonally close–packed (*hcp*) structure[3–7]. The *hcp* structure can coexist with *fcc* as a metastable phase in pure rare gas solids at low temperatures[3–6] and becomes stable in solid solutions[3,8,9]. Calculations based on two– and many–body interaction potentials have predicted the *hcp* structure to be energetically more favorable than the *fcc* polymorph[10,11]. This stability order is reversed after including zero–point vibrational effects[10].

The stability of *hcp* structures is also supported by high–pressure experiments[12–18]. Rare gas solids martensitically transform from *fcc* to *hcp* before metalization under pressure[12–15]. The pressure–induced *fcc*–to–*hcp* transition in RGSs is sluggish as the two phases coexist over a wide range of pressures. X–ray diffraction and Raman spectroscopy show a transformation pressure in the range of 1.5–41 and 3.2–50 GPa for Xe and Kr, respectively, and beyond 49.6 GPa for Ar[12–14,16–18]. Theoretically, sluggishness of the *fcc* to *hcp* transformation in Xe was attributed to high energy barrier[19]. This first–principles study determined the energy barrier for a stacking disorder growth pathway[20] at lower pressure and an alternative pathway involving an orthorhombic distortion at higher pressure.

Recent theoretical and experimental studies[21–23] on free clusters of inert gases investigated the relation between cluster size and the stability of the *hcp* structure. It was shown that increasing the Ar cluster size led to a transition from *fcc* to *fcc*/*hcp* mixed structures. An orthorhombic structure was predicted as intermediate in the *fcc*–to–*hcp* transition. It accounts for the diffraction peaks originating neither in *fcc* nor *hcp* structures in Ar nanoclusters[24]. Although the *fcc*–to–*hcp* transition mechanism was extensively studied for rare gas clusters, a comprehensive understanding of this transformation in the corresponding bulk materials is still elusive.

To answer these questions, we employ Transition Path Sampling[25,26] to provide detailed atomistic understanding of the transition mechanisms and the ensuing structures.

II. SIMULATION DETAILS

For our transition path sampling molecular dynamics simulations we used the TPS module from the USPEX package[27–30] in combination with the LAMMPS code[31]. During sampling, 7427 successful trajectories out of 17334 trial moves were collected and used for analysis. For each trajectory, molecular dynamics was carried out using the velocity–Verlet algorithm with a time step of 0.1 fs to ensure good reversibility. The simulation system employed a Nose–Hoover thermostat with a relaxation time of 30 fs and a Nose–Hoover barostat with a relaxation time of 300 fs, ensuring an NpT ensemble[24] at $T = 40$ K and $P = 1$ bar. Anisotropic shape changes of the simulations box containing 8000 Ar atoms were allowed to avoid biasing the evolution of the dynamics and the resulting transition mechanism. The interatomic interactions were modeled using Lennard–Jones 12–6 model with Ar interaction parameters $\sigma = 3.405$ Å and $\epsilon = 0.238$ Kcal/mole[10,32], and truncated at 10 Å.

The Radial Distribution Function (RDF) can be used as an Order Parameter (OP) to distinguish structures

along the path and compare to the two stable structures. The path is a trajectory connecting the stable states as long as the RDFs of the initial and final structures agree with the *fcc* and *hcp* structure within tolerance, respectively. For the structures along the trajectory, their RDF difference from stable structures indicates their deformation.

The transition path sampling simulations were started by an initial trajectory connecting the *fcc* and *hcp* phases generated by the Variable–Cell Nudged Elastic Band (VC–NEB)[33] method.

III. RESULTS AND DISCUSSIONS

A. Energetic Description of Phase Transition

The enthalpy of the structures along a trajectory yield the energetic description of the transition. Fig. 1(a) shows the enthalpy change of a sample trajectory I across the transition. The energy barrier is about 3.2 meV/atom, slightly lower than the thermal energy (kT = 3.45 meV/atom) at 40 K showing that such a transition is thermally feasible.

By averaging over all accepted trajectories, the enthalpy for *fcc* and *hcp* structures are -69.89 ± 0.06 meV/atom, -69.85 ± 0.03 meV/atom respectively. The peak enthalpy of the transition structures is -66.75 ± 0.05 meV/atom. The energy barrier for *fcc*→*hcp* transition is 3.12 ± 0.07 meV/atom, which is comparable to the thermal energy of 40 K. Despite the low energy barrier per atom, the transition in bulk is expected to be sluggish, waiting for sufficient thermal fluctuations to complete the transition for all atoms. This is further clarified by the definition of the phase transition region and its corresponding transition time.

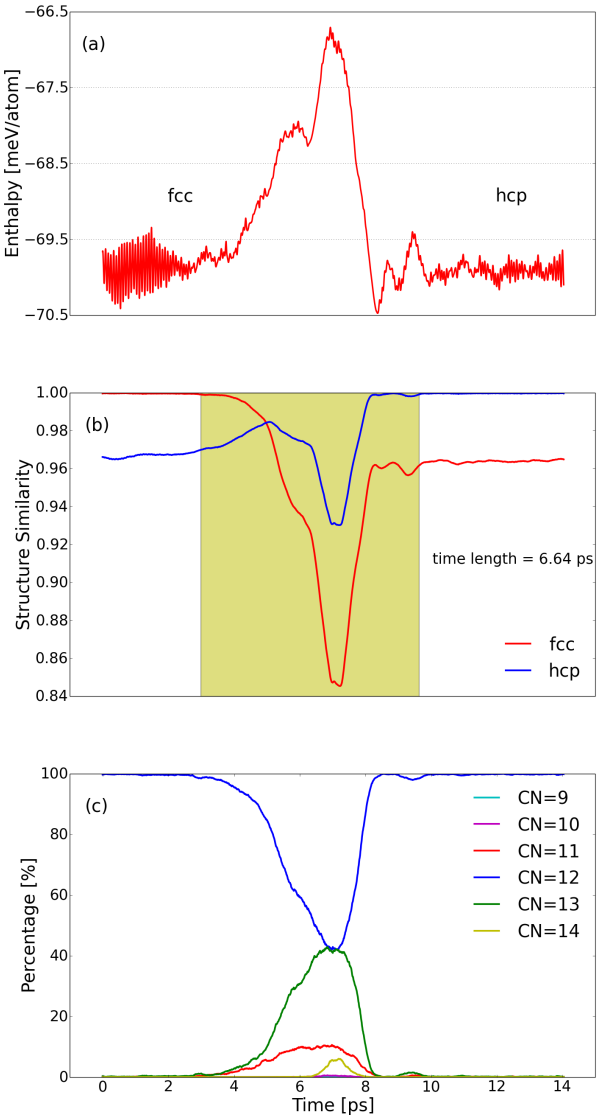

FIG. 1: (a) Enthalpic description of trajectory I. (b) The transition region (yellow) of trajectory I. Structure similarities to *fcc* and *hcp* phases are plotted in red and blue separately. (c) The percentages of differently coordinated atoms along trajectory I.

B. Structural Description of Phase Transition

1. *Characterization of Transition Structures*

The crystal symmetry of the stable phases, *fcc* and *hcp*, is clearly lost during the transformation. Two ways are used here to analyze the deformation of the lattice and the local packing in these structures.

The lattice deformation is measured by the structure similarity to *fcc* and *hcp*. Radial Distribution Functions $g(r)$ are used as a simple but effective description. For the structure x along the transition trajectory, the $g(r)$ values are specified at a set of discrete distances $r = \{r_0, r_1, \ldots, r_n\}$. The corresponding $g(r)$ values form an RDF vector, $\vec{G}_x = [g(r_0), g(r_1), \ldots, g(r_n)]$. Using the previous concept of a fingerprint descriptor[34], the structure x's similarity to *fcc* phase can then be determined with a structure similarity function $S_{fcc}(x)$,

$$S_{fcc}(x) = \frac{\vec{G}_x \cdot \vec{G}_{fcc}}{|\vec{G}_x||\vec{G}_{fcc}|} \tag{1}$$

which is the cosine distance between the RDF vector of structure x and the *fcc* phase. The structure similarity function ranges from 0 meaning totally uncorrelated, to 1 meaning identical; in–between values indicate intermediate similarity. The *fcc*–structure similarity criterion is set to be 0.999, i.e. if $S_{fcc} > 0.999$ we identify a structure as *fcc*. The similarity to the *hcp* phase is defined analogously. With this function, we distinguish the transition

structure from the two stable structures. The transition region can thus be characterized for each trajectory.

Fig. 1(b) indicates the *fcc*→*hcp* transition along trajectory I. The transition begins at 2.99 ps, when the structure loses its similarity to the *fcc* phase beyond the tolerance, and ends at 9.63 ps as the structure gains more than 99.9% similarity to *hcp*. Along trajectory I, it takes 6.64 picoseconds to finish this transition. Note that these times might not be corresponding to real times but can be used to compare dynamics between different trajectories. For all accepted transition trajectories, the average transition time is 7.45 ± 1.17 picoseconds within the cell of 8000 atoms.

The local packing along each trajectory is analyzed through the percentages of differently coordinated atoms. In *fcc* or *hcp* structures, the coordination number of each atom is 12. Over– and under–coordinated atoms appear during the transition.

Fig. 1(c) provides percentages of not–12–coordinated atoms in the structures along trajectory I. After 2.99 ps, the ratio of 12–coordinated atoms decreases. Simultaneously, both over– and under–coordinated atoms, mainly 13–coordinated and 11–coordinated atoms, increase. 14–coordinated atoms only appear briefly; 9– and 10–coordinated atoms are almost negligible. These over– and under–coordinated atoms in Fig. 1(c) represent the production of local defects. The number of these defects reaches its maximum when the 12–coordinated atoms are at their lowest at 6.94 ps. After the 9.63 ps, the local packing in the solid becomes 12-coordinated consistent with the *hcp* phase.

In Fig. 1(b) and Fig. 1(c), it is noticeable that the lattice deforms immediately after the local packing begins to change. The lattice has the maximum local defects and the greatest deformation at the same time, followed by a simultaneous relaxation into stable phase. This consistency is observed in all three types of transition pathways.

2. *Classification of Transition Pathways and the Mechanisms*

We are defining 3 types of transitions. Trajectory I represents a Class I transition. The lattice deforms slowly from the *fcc* phase to the transition state but relaxes quickly to the *hcp* phase. The growth and decay rates of local defects dominate the transformation process. Fig. 1(b) and (c) indicate the consistency between the lattice deformation and local defects. When more than 1.5% atoms become over– or under–coordinated the lattice loses its similarity to *fcc* at 2.99 ps. According to Fig. 1(a) and (c), the increasing enthalpy follows the local packing change since the beginning of transition. When the system reaches the local minimum in energy at 6.25 ps more than 45% atoms are not regularly coordinated. After waiting for sufficient thermal fluctuations to activate further local packing changes, more local defects are generated to accelerate the lattice deformation. When the system has the highest energy and largest number of local defects at 6.94 ps, the structure has least similarity to both *fcc* and *hcp* phase. The lattice afterwards quickly relaxes to the stable *hcp* phase. Although the average arrangement of atoms demonstrates the character of *hcp* at 8.56 ps, the coordination numbers still stabilize to 12 until 9.63 ps in order to dissipate the energetic fluctuations.

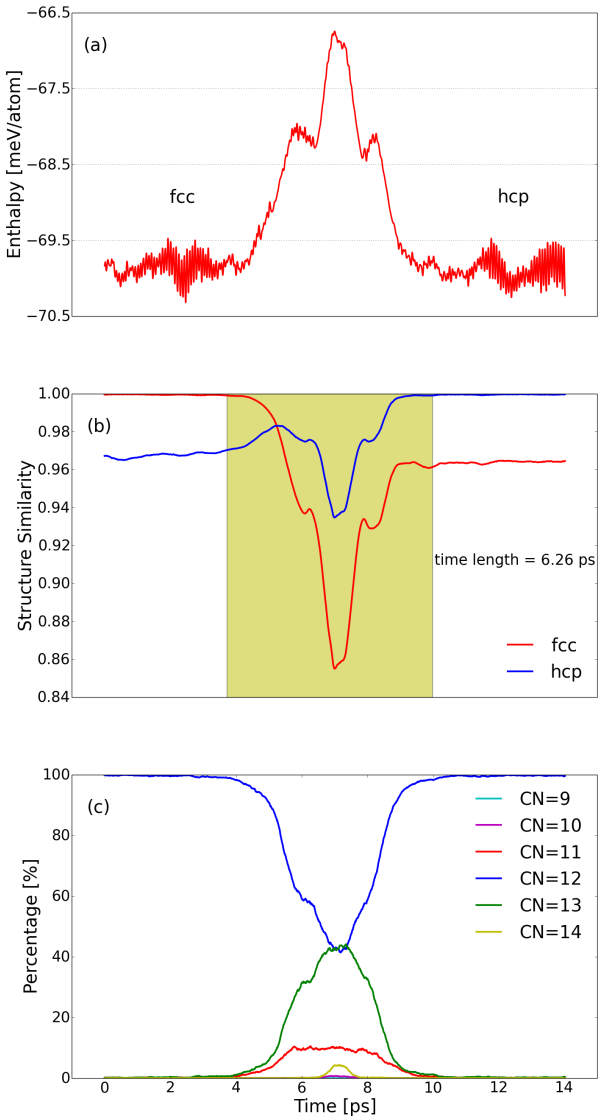

FIG. 2: (a) Enthalpic description of trajectory II. (b) The transition region (yellow) of trajectory II. Structure similarities to *fcc* and *hcp* phases are plotted in red and blue separately. (c) The percentages of differently coordinated atoms along trajectory II.

A Class II transition can be observed in trajectory II. During transition, the lattice deformation and relaxation take almost equal time. Based on the structure similarity, the lattice begins to deform at 3.72 ps and reaches the

largest deformation 3.28 ps later. Then it takes 2.98 ps to relax into the *hcp* phase. As shown in Fig. 2(a), two metastable states appear during the lattice deformation and relaxation. The first metastable state forms at 6.39 ps and soon accumulates thermal energy to produce more local defects, which facilitate the following lattice deformation. After overcoming the transition saddle at 7.00 ps, the lattice is trapped into a second metastable state. But it just takes 0.39 ps to overcome the small energy barrier and quickly relax to the *hcp* phase at 9.98 ps. The shortest pathway of all simulations is also in this transition type, lasting only 3.87 ps.

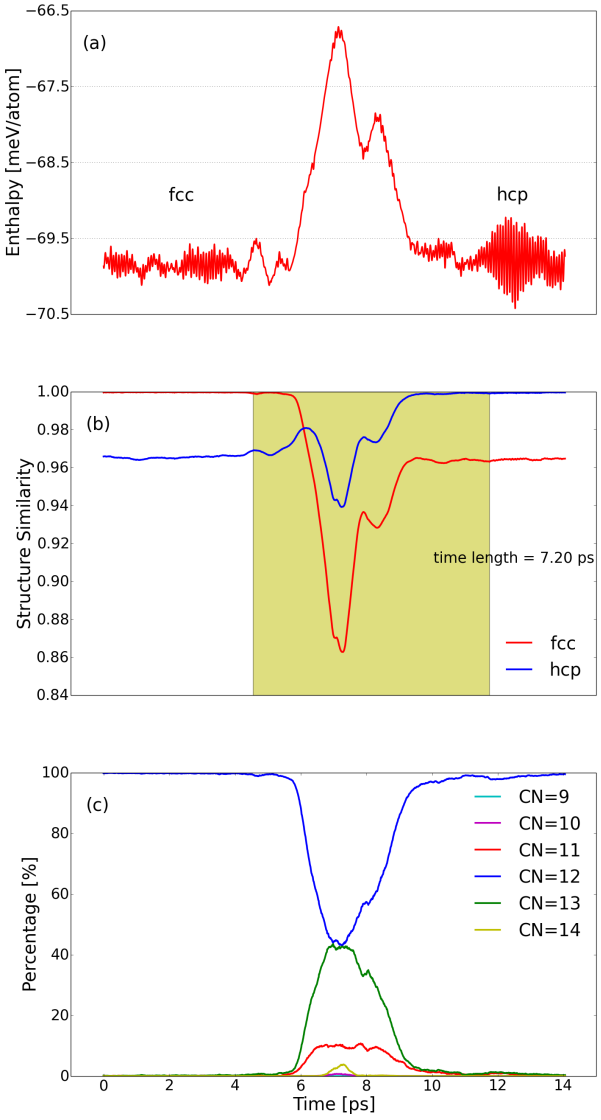

FIG. 3: (a) Enthalpic description of trajectory III. (b) The transition region (yellow) of trajectory III. Structure similarities to *fcc* and *hcp* phases are plotted in red and blue separately. (c) The percentages of differently coordinated atoms along trajectory III.

Fig. 3(b) indicates a Class III transition, in which the lattice experiences a fast deformation and slow relaxation. Starting with a small thermal fluctuation at 4.55 ps, only 2% of atoms becomes not–12–coordinated until 5.66 ps. The structure still demonstrates 99.8% similarity to *fcc*. However, induced by a large fluctuation from that moment, the lattice experiences a rapid change. More than 55% atoms lose their regular coordination numbers within 1.6 ps. As a result, the transition state has the largest deformation from both *fcc* and *hcp* phases at 7.26 ps. A following increase of 12–coordinated atoms reduces the local defects and leads to metastable phase with more structural similarity to *hcp* phase at 7.91 ps. Another 0.51 ps is required to overcome the energy barrier. The lattice relaxation to *hcp* is completed at 11.75 ps. The whole transition length characterized through the structure similarity is 7.20 ps.

Looking at enthalpy profiles of three transformation paths presented above, we can see that their activation enthalpies are identical. From the enthalpy viewpoint alone one could conclude that these paths have equal chances to occur in reality, but this would ignore the entropic factor. A simple and effective way to judge the likelihood of occurrence of each path, taking entropic factor into account is to count the frequency of occurrence of each type of pathway. We find that the percentage of class I is 25.6%, class II is 13.0%, class III is 61.4% and we therefore assume that class III is the most likely but the other ones have a significant share.

C. Type of Phase Transformation

For trajectory I, the distribution of differently coordinated atoms along the transition is given in Fig. 4. At the beginning, nearly all atoms in the *fcc* structure are 12–coordinated. The lattice is characterized by a stacking sequence $\ldots ABCABC\ldots$. Although the lattice deformation starts at 2.99 ps, the coordination numbers stay at 12 for more than 80% atoms until 5.18 ps. When the thermal fluctuation brings the system into a metastable phase at 6.25 ps, more than 45% atoms become over– or under–coordinated. After a short time, the system reaches the peak in enthalpy at 6.94 ps with the most changes to atomic coordination numbers. The generation of sufficient defects in this process facilitates the following lattice relaxation. After the largest deformation, the structure quickly relaxes to *hcp* by 8.56 ps. But only at 9.63 ps all atoms again are 12–coordinated. The whole system ends with the *hcp* phase at 14 ps with a stacking sequence of $\ldots ABABAB\ldots$.

As observed in Fig. 4, the over– and under–coordinated atoms appear in neighboring regions and these regions form uniformly throughout. This initial step of the transition is similar for the other two classes. It is noticeable that the lattice deformation is changed consistently with the local packing. There is cooperative movement of many atoms that results in the *fcc* stacking growth into *hcp* domains and the final change in crystal struc-

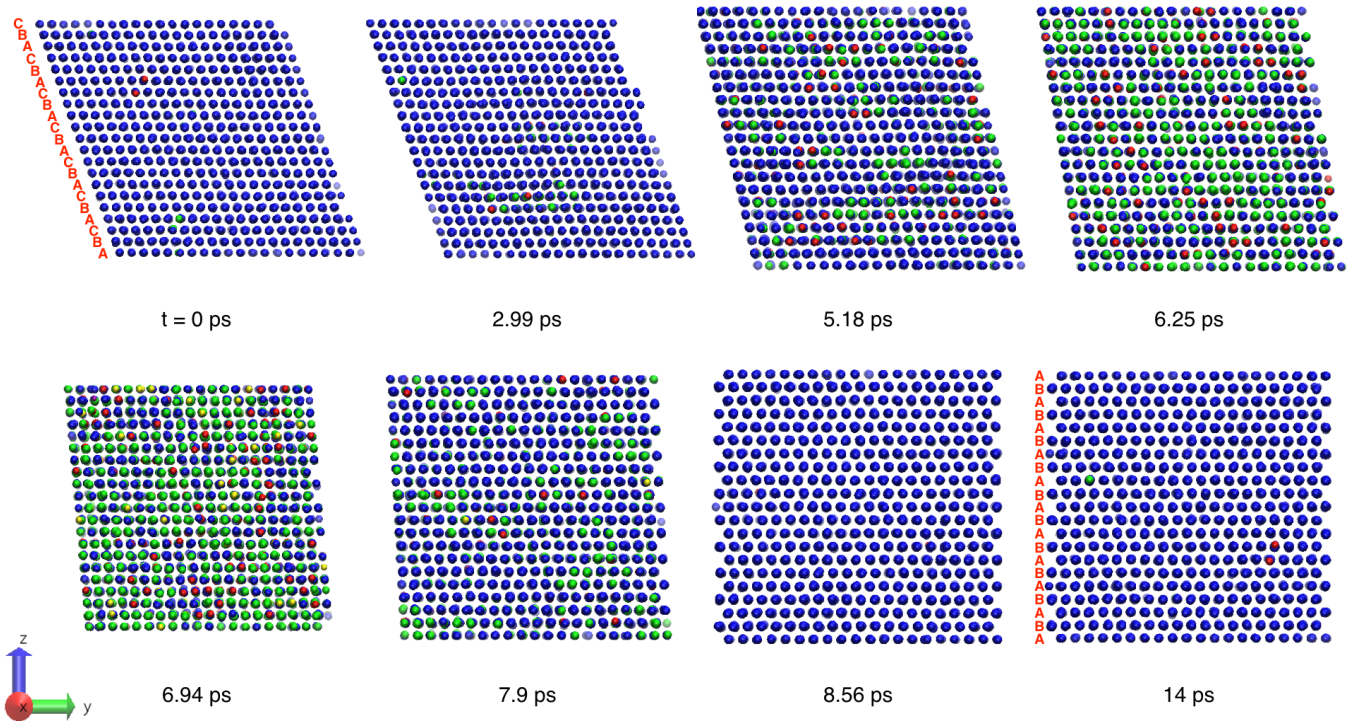

FIG. 4: Snapshots of configurations during a transition, different colors are different coordination numbers. Atoms in blue are 12–coordinated while red and green are for 11– and 13–coordinated atoms.

ture. The stacking disorder growth mechanism was previously observed in experimental studies of *fcc*–to–*hcp* transition of Xe and Kr[13,20]. A first–principles calculation suggested this mechanism as the transition pathway in Xe at lower pressure[19]. An X–ray diffraction study on solid Ar up to 114 GPa predicted the development of stacking disorder during the transition[14]. However, there is still not enough evidence to prove this assumption as the *fcc*–to–*hcp* transition in Ar requires extreme compression above 49.6 GPa[12–14,16–18]. Our previous results about the high energy barrier explains the inaccessibility of this transition in bulk at ambient conditions.

IV. CONCLUSIONS

Our results show that the transition energy barrier is at the level of thermal energy for each atom to complete *fcc*–to–*hcp* transformation in solid Ar at 40 K under ambient pressure. However, the activation energy required for this transformation in bulk is beyond thermal fluctuations. Our average transition times are short in a cell of 8000 atoms, it will take much longer in real–sized samples. This is evidenced by experimental observations of fast transitions in cluster but sluggish even unobservable transition in bulk[12–18,21–24,35]. Structural analysis in physical time demonstrates three different transition pathways. These pathways all indicate the formation of over– and under–coordinated atoms, which lie in neighboring regions and distribute uniformly through the whole lattice. Unlike the transition in Ar clusters[24] no orthorhombic intermediate is observed. Instead, we find a stacking disorder growth mechanism featured by the collective movement of atoms and stacking sequence change of lattice during transition. It is worth mentioning that class III has the lowest number of not–12–coordinated atoms and the least lattice deformation. We cannot exclude that there might be some nucleation induced pathways as well available to the systems although we could not identify a nucleus in any of our simulations.

The homogeneous growth of *hcp* phase from *fcc* phase requires sufficient transition time for atoms to cooperatively overcome high energy barrier and transform to the *hcp* phase. This phenomenon further explains the sluggishness of *fcc*–to–*hcp* transformation in bulk Ar and the missing observation of this bulk transition at lower temperature without extreme compression.

The TPS method employed in our research provides a precise atomic understanding of Ar phase transition. Our results confirm the experimental observations with theoretical support. Clearly, TPS can be extended to investigate the martensitic transformation mechanism of rare gas solids under high pressure, which would be a significant advantage over previous studies[19]. We are confident that the combination of experiments and computation is a stimulating way to develop detailed insights into future

phase transition problems.

* bxli@ucdavis.edu
† rfaller@ucdavis.edu

[1] T. Barron and C. Domb, in *Proceedings of the Royal Society of London A: Mathematical, Physical and Engineering Sciences*, Vol. 227 (The Royal Society, 1955) pp. 447–465.
[2] L. Jansen, Physics Letters **4**, 91 (1963).
[3] L. Meyer, C. Barrett, and P. Haasen, The Journal of Chemical Physics **40**, 2744 (1964).
[4] C. Barrett and L. Meyer, The Journal of Chemical Physics **41**, 1078 (1964).
[5] E. Schuberth, M. Creuzburg, and W. Müller-Lierheim, physica status solidi (b) **76**, 301 (1976).
[6] Y. Sonnenblick, E. Alexander, Z. Kalman, and I. Steinberger, Chemical Physics Letters **52**, 276 (1977).
[7] B. W. van de Waal, Phys. Rev. Lett. **67**, 3263 (1991).
[8] N. Galtsov, A. Prokhvatilov, and M. Strzhemechnyı, Low temperature physics **30**, 984 (2004).
[9] A. Curzon and M. Eastell, Journal of Physics C: Solid State Physics **4**, 689 (1971).
[10] P. Schwerdtfeger, N. Gaston, R. P. Krawczyk, R. Tonner, and G. E. Moyano, Physical Review B **73**, 064112 (2006).
[11] N. Krainyukova, Low Temperature Physics **37**, 435 (2011).
[12] D. Errandonea, B. Schwager, and R. Boehler, International Journal of High Pressure Research **22**, 375 (2002).
[13] D. Errandonea, B. Schwager, R. Boehler, and M. Ross, Physical Review B **65**, 214110 (2002).
[14] D. Errandonea, R. Boehler, S. Japel, M. Mezouar, and L. Benedetti, Physical Review B **73**, 092106 (2006).
[15] A. Jephcoat, H.-k. Mao, L. Finger, D. Cox, R. Hemley, and C.-s. Zha, Physical review letters **59**, 2670 (1987).
[16] H. Shimizu, N. Wada, T. Kume, S. Sasaki, Y. Yao, and J. S. Tse, Phys. Rev. B **77**, 052101 (2008).
[17] Y. A. Freiman, A. F. Goncharov, S. Tretyak, A. Grechnev, S. T. John, D. Errandonea, H.-k. Mao, and R. J. Hemley, Physical Review B **78**, 014301 (2008).
[18] H. Shimizu, M. Kawajiri, T. Kume, S. Sasaki, Y. A. Freiman, and S. M. Tretyak, Phys. Rev. B **79**, 132101 (2009).
[19] E. Kim, M. Nicol, H. Cynn, and C.-S. Yoo, Physical review letters **96**, 035504 (2006).
[20] H. Cynn, C. Yoo, B. Baer, V. Iota-Herbei, A. McMahan, M. Nicol, and S. Carlson, Physical review letters **86**, 4552 (2001).
[21] O. Danylchenko, S. Kovalenko, and V. Samovarov, Low Temperature Physics **30**, 166 (2004).
[22] A. Danilchenko, S. Kovalenko, and V. Samovarov, Low Temperature Physics **34**, 966 (2008).
[23] O. Danylchenko, S. Kovalenko, O. Konotop, and V. Samovarov, Low Temperature Physics **40**, 1083 (2014).
[24] N. Krainyukova, R. Boltnev, E. Bernard, V. Khmelenko, D. Lee, and V. Kiryukhin, Physical review letters **109**, 245505 (2012).
[25] P. G. Bolhuis, D. Chandler, C. Dellago, and P. L. Geissler, Annual review of physical chemistry **53**, 291 (2002).
[26] C. Dellago, P. G. Bolhuis, and P. L. Geissler, in *Computer Simulations in Condensed Matter Systems: From Materials to Chemical Biology* (Springer, 2006) pp. 349–391.
[27] C. W. Glass, A. R. Oganov, and N. Hansen, Computer Physics Communications **175**, 713 (2006).
[28] A. R. Oganov, A. O. Lyakhov, and M. Valle, Accounts of chemical research **44**, 227 (2011).
[29] A. O. Lyakhov, A. R. Oganov, H. T. Stokes, and Q. Zhu, Computer Physics Communications **184**, 1172 (2013).
[30] S. E. Boulfelfel, A. R. Oganov, and S. Leoni, Scientific reports **2**, 471 (2012).
[31] S. Plimpton, Journal of Computational Physics **117**, 1 (1995).
[32] J. Hirschfelder, C. Curtis, and R. Bird, Wiley, New York (1964).
[33] G.-R. Qian, X. Dong, X.-F. Zhou, Y. Tian, A. R. Oganov, and H.-T. Wang, Computer Physics Communications **184**, 2111 (2013).
[34] A. R. Oganov and M. Valle, The Journal of chemical physics **130**, 104504 (2009).
[35] E. Verkhovtseva, I. Gospodarev, A. Grishaev, S. Kovalenko, D. Solnyshkin, E. Syrkin, and S. Feodosev, Low Temperature Physics **29**, 386 (2003).